

Stretching single atom contacts at multiple subatomic step-length†

Cite this: *Phys. Chem. Chem. Phys.*, 2013, **15**, 12459

Yi-Min Wei,^a Jing-Hong Liang,^a Zhao-Bin Chen,^a Xiao-Shun Zhou,^b Bing-Wei Mao,^{*a} Oscar A. Oviedo^c and Ezequiel P. M. Leiva^{*c}

Received 1st February 2013,
Accepted 26th March 2013

DOI: 10.1039/c3cp50473e

www.rsc.org/pccp

This work describes jump-to-contact STM-break junction experiments leading to novel statistical distribution of last-step length associated with conductance of a single atom contact. Last-step length histograms are observed with up to five for Fe and three for Cu peaks at integral multiples close to 0.075 nm, a subatomic distance. A model is proposed in terms of gliding from a *fcc* hollow-site to a *hcp* hollow-site of adjacent atomic planes at 1/3 regular layer spacing along with tip stretching to account for the multiple subatomic step-length behavior.

1. Introduction

Quantum transport of electrons through metallic nanocontacts has attracted continuous interest in both experiment and theory since Landauer's formula for evaluation of conductance of metallic atomic contact was proposed.¹ Research on this topic has recently been stimulated by an increasing desire for the miniaturization of electronic devices, including molecular-based devices, and has benefited from the rapid development of experimental techniques to form nanocontacts.^{2–4} By employing well-established techniques such as the mechanically controllable break junction (MCBJ)^{5–9} and the scanning probe microscope breaking junction (SPM-BJ),^{6,10–14} metallic nanocontacts can be formed and then elongated to break, repeatedly, so that conductance traces can be monitored down to a single atom contact.

Several groups have described how information about atomic rearrangement during the stretching of a nanocontact can be extracted by statistical analysis of plateau lengths (*i.e.* step lengths) of stepwise conductance traces.^{6,8,15,16} Since the length of the last conductance plateau corresponds to the stretching at single atom contacts, it can only be related to

the structural deformation at the single atom contact, and this can be influenced by the crystallography of the nanocontact. Several groups have reported structural evolution of a single atom contact at low temperature and in ultra high vacuum conditions.^{6,8,17,18} Typically, the lowest peak of the last-step length histogram locates at around 0.2 to 0.3 nm, which is on the atomic scale and corresponds to single atom addition at the contact in the stretching direction. A room temperature study was also reported by using conducting atomic force microscopy, in which conductance histograms with three integer multiples of subatomic distance were obtained.¹⁹

However, reliable statistical analyses of last-step length of conductance traces rely on the control of the structure of the nanocontacts over the whole set of experiment, which is experimentally challenging. Therefore, considerable deviation in the structure of nanocontacts may exist compared to those considered in theoretical simulations,^{20–26} where a well-defined structure of the nanocontact is assumed. Conventional MCBJ as well as SPM-BJ are based on random mechanical crashing to form nanocontacts, and thus control over the structure of the nanocontacts is not ensured. Even for nanocontacts that are formed by electromigration,^{27,28} in which a high electric field is applied to promote atomic migration and thus induce deformation of the metallic nanowire, real time high resolution transmission electron microscopic (HRTEM)^{29–33} observation of structural evolution at the nanocontact reveals additional unexpected complexity. In this case, the complication could also arise from the exposure of the nanocontact under irradiation of electron beams with additional effects including localized charging and heating.^{15,34,35} Pure electrodeposition onto the two counter-facing electrodes of a nanogap may be a way to create nanocontacts through natural and delicate touching,^{36–39} and some

^a State Key Laboratory of Physical Chemistry of Solid Surfaces and College of Chemistry and Chemical Engineering, Xiamen University, Xiamen 361005, Fujian, China. E-mail: bwmiao@xmu.edu.cn; Fax: +86 592 2186862; Tel: +86-592 2183047

^b Zhejiang Key Laboratory for Reactive Chemistry on Solid Surfaces, Institute of Physical Chemistry, Zhejiang Normal University, Jinhua 321004, Zhejiang, China

^c Departamento de Matemática y Física – INFIQC, Facultad de Ciencias Químicas, Universidad Nacional de Córdoba, Ciudad Universitaria, X5000HUA Córdoba, Argentina. E-mail: eleiva@fcq.unc.edu.ar

† Electronic supplementary information (ESI) available: Calibration of stretching speed; statistical analysis of step-length and last-step histogram; simulation for Cu growth on Au(111). See DOI: 10.1039/c3cp50473e

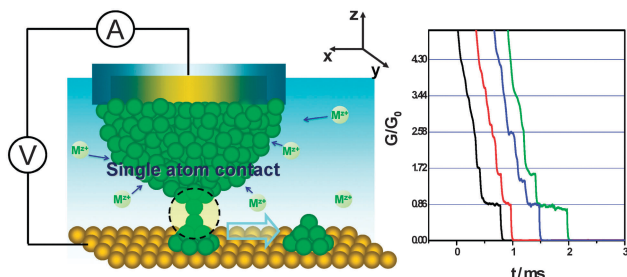


Fig. 1 Schematic illustration of the electrochemistry-assisted jump-to-contact STM-BJ approach for creating the nanocontact (left). Typical conductance traces of Fe recorded during the stretching of the atomic contact (right). Metallic clusters are left as side products on the surface following rupture of the contact.

crystallography-related features have been observed.³⁷ However, the control of the nanocontact seems to be less flexible by electrodeposition alone because of the difficulty in attaining balanced kinetics of electrodeposition. Very recently, STM-BJ experiments conducted in UHV by Sabater *et al.* have shown that provided the indentation depth is limited up to a conductance value of approximately $5 G_0$, where $G_0 = 2e^2/h$, atomically well-defined contacts can be obtained by repeated formation and rupture of the nanocontacts between two gold electrodes.⁴⁰

Recently, we have developed an electrochemically-assisted jump-to-contact STM-BJ approach in an electrochemical environment,⁴¹ Fig. 1. The metal of interest is electrochemically deposited onto the tip and formation of the metal nanocontact is achieved by chemical interaction⁴² of the metal with the substrate surface so that the tip is only gently contacting the substrate. This extends the generality of STM-BJ in terms of the variety of not only metallic but also molecular junctions with various metal electrodes. Nanocontacts such as Fe, Pd, Cu⁴¹ and Ag,⁴³ as well as molecular junctions using Ag and Cu⁴⁴ as electrodes, have been successfully constructed and their conductances measured. Such measurements were otherwise hard to perform under ambient conditions. Furthermore, it has been demonstrated in our previous work⁴³ that Ag nanocontacts created by the electrochemically-assisted jump-to-contact STM have integral conductance in units of G_0 with that at $2 G_0$ most abundant.⁴³ This is in agreement with a theoretical prediction based on a well-defined contact structure, but in contrast to the fractional conductance of the contact measured by conventional STM-BJ approach, suggesting that it is feasible to obtain a well-defined contact structure by jump-to-contact based STM-BJ. A further distinct feature of the jump-to-contact STM-BJ approach is the controlled location at which each break junction measurement is made and a cluster on breaking each contact is created. This means that each measurement is independent of the history of measurement, and this is highly desirable for practical as well as theoretical considerations.

In this paper, we demonstrate that by using the jump-to-contact approach of STM-BJ with well-defined crystallographic control of nanocontacts, information about the structural evolution during stretching of a nanocontact to a single atom contact can be obtained. Well-defined multiple peaks of stretching length distributions at single atom contacts of both Fe and Cu are

observed with peaks at integral multiples of a distance considerably smaller than their atomic radii. The observation shines light on the experimental investigations of crystallographic correlation of the mechanical and transport properties of nanocontacts, in harmony with theoretical simulation.

2. Experimental section

In Fig. 1, the tip is continuously loaded with the Fe or Cu by electrochemical deposition before, during, and after contact formation. To drive the tip towards the surface, an externally controlled voltage pulse of several tenths of a volt is superimposed onto the Z-piezo of the STM scanner with the feedback circuit enabled but with lower integral and proportional gains, *e.g.* 0.1, than used for imaging. When the tip is driven very close to the substrate, a jump-to-contact process is induced resulting in metal atom transfer from the apex of the tip to the substrate to create a nanocontact. This is accompanied by an immediate and dramatic rise in current which is detected by the STM feedback circuit and results in tip withdrawal. This stretches the nanocontact down to a single atom bridge which eventually ruptures with a cluster of metal atoms being formed on the surface.^{45,46} The duration of the external voltage pulse is set at a scale of several milliseconds, sufficiently long for STM feedback to respond up to rupture of the nanocontact. The response of the STM Z-piezo voltage on application of the external voltage pulse shows an essentially linear relationship with time during the stretching step, giving a fixed stretching rate of $1.3 \pm 0.1 \mu\text{m s}^{-1}$, Fig. S1 (ESI[†]). During the stretching stage, the conductance of the nanocontact is continuously monitored and recorded to generate conductance traces. The process is repeated thousands of times, each at a new location, so that an array of clusters is formed after measurement. Statistical analysis of thousands of such conductance traces was performed, Fig. S2 (ESI[†]). A last-step length histogram was constructed, which reveals the statistical probability of the stretching length at single atom contact.

Conductance measurements and *in situ* STM characterization were carried out on a modified Nanoscope E STM (Veeco, Santa Barbara, CA) under constant-current mode. To match the measuring range of the quantized conductance of metallic nanocontacts, the current preamplifier of STM was adjusted to 5556 nA V^{-1} , less sensitive than the value normally used for imaging. Mechanically cut Au tips were used after being insulated by thermosetting polyethylene to reduce the Faradaic current. Platinum wire was used as the counter electrode and Ag/AgCl and Cu wire as reference electrode in the system for Fe and Cu, respectively.

Electrodeposition and nanocontact fabrication of Cu and Fe were carried out in aqueous and in 1-butyl-3-methylimidazolium tetrafluoroborate (BMIBF₄) ionic liquid,^{47,48} respectively, on both Au(111) and Au(100). Further details can be found elsewhere.⁴¹

3. Results and discussions

Experimental verification of crystallographic features of Fe clusters formed on the surface after rupture of the single atom

contact has been performed by monitoring the growth behavior of the clusters. Shown in Fig. 2(a and b) are 10×10 arrays of Fe clusters created on both Au(111) and Au(100) by STM jump-to-contact processes. The clusters are several nanometers in diameter and two to three atomic layers in thickness. They were allowed to grow further at a small overpotential (*i.e.* slightly more negative than the equilibrium potential). The morphology of Fe clusters changes to show unique pseudo-rod like and pseudo-square like structures on Au(111) and Au(100), respectively, which has been found to be characteristic of Fe electrodeposition on the respective surfaces.⁴⁹ Although one-to-one identification of the original cluster is not possible because of the overlap between the growing anisotropic structures and interference of growth from the cluster-free area, the protrusions of the deposit in the cluster region indicate enhanced growth at the clusters, which actually serve as growth centers. Obviously, the anisotropic growth behavior only could be preserved and observed in this region when the clusters are epitaxial with the surface structure.

Molecular dynamics (MD) simulations have been performed to generate STM tip-induced clusters of Cu. This methodology has been found useful to understand cluster formation in STM-break junction experiments.^{50–53} The present results have revealed a gradual atomic rearrangement of the corresponding nanocontacts to accommodate their structure epitaxially with the substrate surface. These results will be published elsewhere. Furthermore, Grand Canonical Monte Carlo (GCMC) simulations

performed on the clusters generated in these MD runs show that their growth follows the orientation of the underlying substrate. Sample results of these simulations are shown in Fig. S3 (ESI†) for Cu deposition on Au(111), and similar results have been obtained for Cu deposition on Au(100). Simulation for Fe is still very difficult because of its complicated electronic structure. However, we expect that these conclusions can be generalized to Fe as well as to other relevant metals.

The well-defined crystalline nature of the clusters as well as the results of computational simulations leads us to propose that nanocontacts constructed on a specified substrate are of a similar structural configuration. This feature has considerable impact on the step-length behavior of conductance traces. Indeed, for both Fe and Cu nanoconstrictions, several sharp peaks were observed on last-step length histograms constructed from 16 000 conductance curves. They locate at almost exact multiples of 0.075 nm as shown in Fig. 3(a) and (b), respectively. The conductance curves were collected in ten segments, each of 1600 curves being associated with formation of a 40×40 array of Fe clusters. The peak intervals are much shorter than the atomic distances of the corresponding metals, yielding values that are hitherto unprecedented in the literature. It is noteworthy that the stretching length of 0.075 nm is just above the noise level of our measurement system, which is *ca.* 0.05 nm. However, after accumulation of 16 000 conductance curves the noise is averaged out so that the three peaks can safely be attributed to the real fluctuation of the measuring system itself. This is verified by examining the histograms with each addition of 1600 curves, and results indeed show gradual build up of the multiple step-length signals, Fig. S5 (ESI†). In fact, a smaller number of conductance traces, *e.g.* 1600 conductance traces already show such last-step length distribution in good experimental conditions. This is in contrast to the usually observed broad distribution of the last-step length at around 0.2 nm reported in literature for *e.g.* Pt and Pd.¹⁸

Two additional control experiments were performed. The first one involved Au nanocontacts, which were fabricated by conventional STM-BJ using an Au tip and Au(111) substrate. For simplicity, the control of the tip movement followed the same procedure as for Cu and Fe, but since no foreign metal was deposited onto the Au tip a slightly higher Z-pulse voltage was applied, which induced mechanical crashing between the tip and the substrate. The last-step length histogram of Au nanocontacts is shown in Fig. 4a, where three peaks, now positioned around 0.33 ± 0.02 nm and their multiple values are clearly observed. The second control experiment involved Cu nanocontacts fabricated also by the conventional STM-BJ approach but associated with film deposition first demonstrated by Murakoshi's group^{38,54} and then Tao's group.⁵⁵ Deposition of a large amount of Cu generates thin film electrodes of Cu on both the tip and substrate. With feedback disabled, the Cu tip was manipulated in the Z direction entirely by the external control voltage. Again, the step-length histogram of the Cu nanocontact showed only one broad peak around 0.18 ± 0.02 nm close to one atom distance, Fig. 4b.

The two control experiments presented above clearly indicate that using the conventional STM-BJ approach, only broad last-step

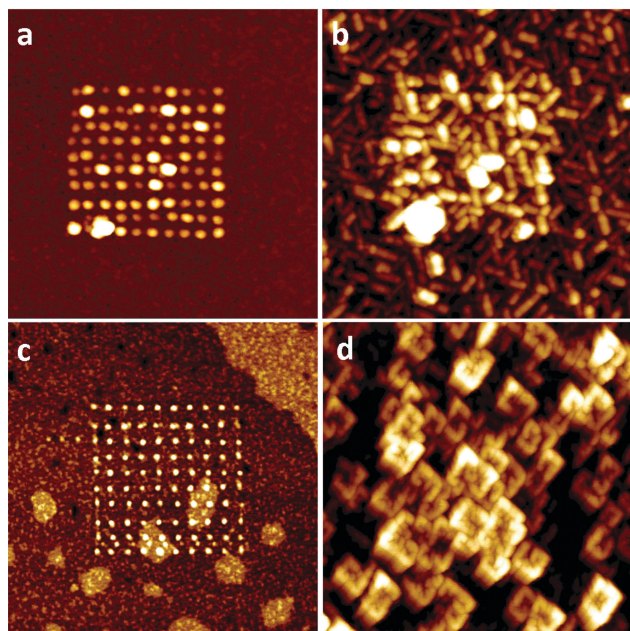


Fig. 2 Single crystalline growth pattern of Fe clusters. (a and c) Clusters formed by jump-to-contact STM on Au(111) and Au(100), respectively; the Au tip and substrate were controlled at -0.8 and -0.75 V vs. Ag/AgCl, respectively, with a typical Z-pulse voltage of 0.45 V. (b and d) Growth of the clusters at -0.95 and -1.05 V on Au(111) and Au(100), respectively; an ionic liquid of 1-butyl-3-methylimidazolium tetrafluoroborate (BMIBF₄) containing ~ 50 mM of dissolved FeCl₃ was employed at room temperature. Scan size for all images: 150×150 nm².

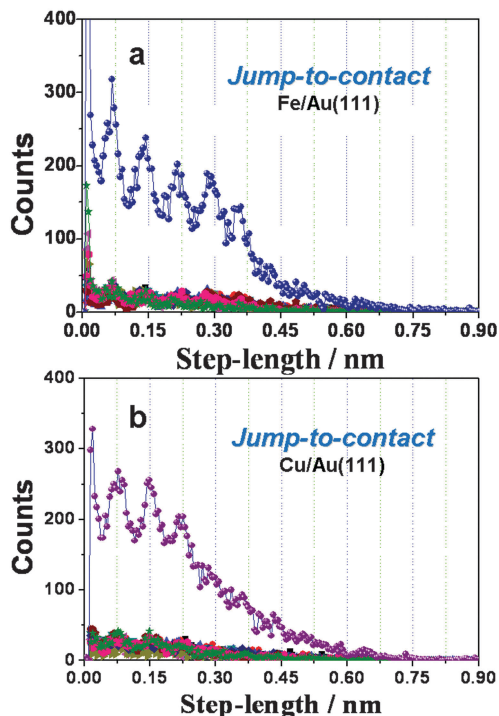


Fig. 3 Last-step length histogram of 16 000 conductance curves (from ten sets of 1600 curves) of Fe (a, blue) and Cu (b, purple) atomic contacts using Au(111). Histograms of the ten sets of conductance curves are also provided for Fe and Cu, which appear in the bottom part of (a) and (b), respectively. The condition for nanoconstriction fabrication of Fe was the same as in Fig. 2(a and c). For Cu, the experiment was performed in an aqueous solution of 1 mM CuSO_4 + 50 mM H_2SO_4 and the Au tip was controlled at -50 mV vs. Cu wire while the Au(111) substrate was controlled at potentials slightly positive with respect to the equilibrium potential for Cu deposition.

length distributions can be observed even with a large number (16 000) of conductance traces. This evidence indirectly supports our hypothesis that the crystallographic characteristics involved during the formation and stretching of nanocontacts by jump-to-contact based STM-BJ are substantially different from those by the conventional mechanical crashing based STM-BJ.

The correlation of last-step length distribution and configuration transition of the nanocontacts is further revealed by careful analysis of the evolution of conductance traces. Taking the Fe nanocontacts as an example, their conductance traces can be divided into two groups. The first group consists of those that show the presence of the second-last-step of conductance at around the first multiple of the last-step conductance (typically in the range of 1.20 – $1.82 G_0$), Fig. 5a. In other words, atomic contacts are stretched, experiencing a two-atom contact before reaching the single atom contact. Therefore, the configuration of the contact changes more smoothly, and a well-defined distribution of last-step length with a satisfactory Gaussian fitting is obtained, Fig. 5c. In contrast, the second group consists of the conductance traces which show high quality last-step plateaus but without the presence of clear or sufficiently long-lived second-last-step of conductance, Fig. 5b. A more abrupt transition to a single atom contact is expected in this case. Accordingly, an ill-defined last-step length distribution is observed without clear distinction of the

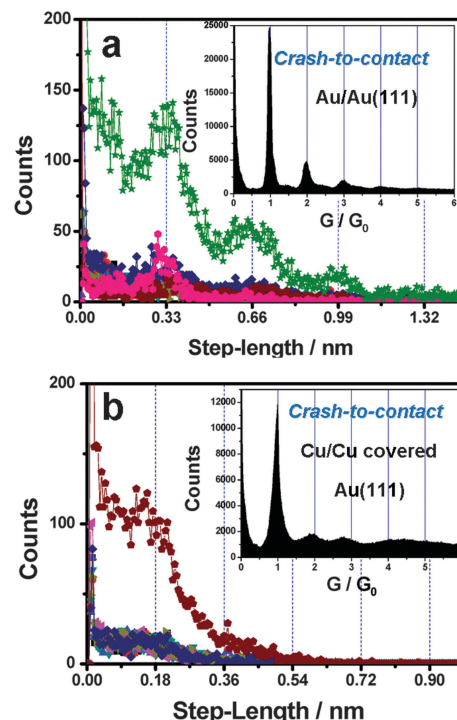


Fig. 4 (a, green) Last-step length histogram of 16 000 conductance curves (from ten sets of 1600 curves) of the Au–Au nanocontacts fabricated in blank BMIBF₄ ionic liquid with a bare Au tip and Au(111) substrate with the procedure of the electrochemistry-assisted STM-BJ system described in previous experiments, but with the higher Z-piezo pulse of 0.8 V. (b, brown) Last-step length histogram of 7000 conductance curves (from seven sets of 1000 curves) of Cu–Cu nanocontacts fabricated by conventional STM-BJ approach when the tip and substrate were both covered by a deposited Cu film with $E_{\text{tip}} -100$ mV, $E_w -50$ mV, and stretching rate 1200 nm s^{-1} . Last-step length histograms of the ten and seven sets of conductance curves of Au and Cu are also provided, which appear in the bottom parts of (a) and (b), respectively. Insets are the corresponding conductance histograms.

multiple peaks, but accompanied by several accessory peaks, Fig. 5d. Based on the discrepancy in the characteristics of conductance traces and resulting last-step length histogram, we expect that a gradual and fine structural transition with high consistency is responsible for the appearance of the remarkably well-defined and multi-peaked distribution of the last-step length in Fig. 5a.

Fe has a more complicated electronic structure near the Fermi level, and theoretical studies^{20,21} have indicated that the conductance of the Fe nanocontact is sensitive to the contact geometry (e.g. Fe single atom or dimer contact). A random displacement from an ideal contact by 0.05 times the lattice constant along the $[001]$ direction would result in a broad histogram of channel transmission.²⁰ Thus, the structural transition associated with a last-step-length of 0.075 nm can be related neither to the metallic bond elongation nor to the geometric displacement at the ideal single atom contact, Fig. 6. Otherwise this would cause conductance changes in the last-plateau of the conductance trace. A reasonable explanation would be a stepped geometrical displacement of the region underpinning the ideal single atom contact.

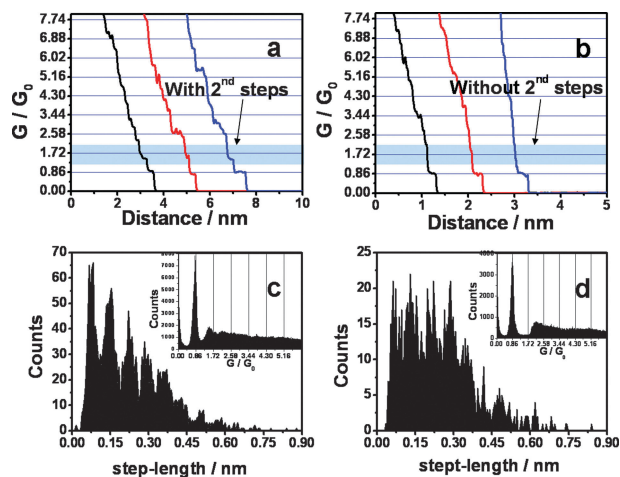


Fig. 5 Typical conductance traces of Fe nanocontacts (a) with both the last and the second-last steps and (b) with last step but without the secondary step. (c) and (d) are the last-step length histograms formed by 2389 and 1064 conductance traces, and corresponding to (a) and (b), respectively. The inserts of (c) and (d) are the corresponding conductance histograms of these two groups.

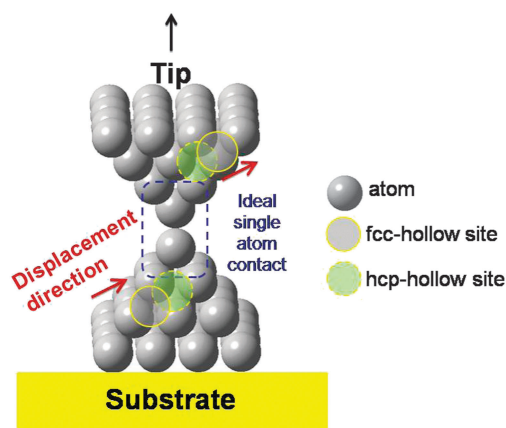


Fig. 6 Schematic illustration of gliding of atomic planes in the contact region with displacement of atoms from e.g. *fcc*-hollow-site to the nearest *hcp*-hollow-site. The ideal single atom contact region outlined by a blue dot square is not involved in the stretching.

It is necessary to mention that in an electrochemical environment, the exact conductance as well as step-length of a single atom contact may be influenced by factors such as density and polarity of the surface charge and adsorption of solvent and ions.⁵⁶ However, an important fact to emphasize here is the observation of the multiple peaks on the conductance histogram of the last-step length at single atom contact, and the stretching distance of *ca.* 0.075 nm happens to be very close to the vertical displacement between the *fcc*-hollow-site and nearest *hcp*-hollow-site of close packed (111) plane of Fe or Cu surface, which is 1/3 of the regular layer spacing. The layer spacing for the (111) plane of Fe and Cu is 0.214 and 0.220 nm, respectively, and thus the vertical displacement would be 0.072 and 0.073 nm, respectively. Therefore, a reasonable explanation for the appearance of the multiple peaks of last-step length

distribution could arise from the gliding of one of the {111}-equivalent planes in the contact region with a displacement of atoms from the *fcc*-hollow-site to the nearest *hcp*-hollow-site upon tip stretching, Fig. 6. Sliding of atomic planes has been proposed by Marszalek *et al.*¹⁹ in which elongation of gold nanowires is at an integer multiple of 0.176 nm, corresponding to 2/3 of the Au regular layer spacing distance. However, gliding with 2/3 of the Fe and Cu regular layer spacing, corresponding to *hcp*- to the nearest *fcc*-site in the stretching direction, Fig. 6, seems not the elemental step in the present work. The gliding processes involving 1/3 layer spacing displacement could benefit from the increased ductility of metals at the nanoscale⁵⁷ because the clusters at the contact involve only a few atomic layers.

Since the gliding can arise from either side next to the ideal single atom contact, multiple values of the stretching distance are possible and indeed up to five (for Fe) or three (for Cu) peaks appear. As the crystallographic feature is expected to be less well-defined on the tip side of the contact, the gliding of atomic planes in the two sides of the contact would be expected to be asymmetric, resulting in an absence of the sixth and fourth last-step length distribution for Fe and Cu, respectively. In addition, since close packed planes are low-energy gliding planes, the {111}-equivalent planes would serve as the most probable gliding planes regardless of the crystallographic orientation of the contacting clusters dictated by the substrate crystallography. Therefore, similar multiple subatomic step-length behavior are observed for both the Au(111) and (100) substrate, showing the generality of the ultrafine structural evolution upon tip stretching. The reduced number of the last-step length for Cu could be explained from its reduced ability in deformation. This is more obvious for the contact formed with the Au(100) surface, where the relative intensity of the second and third peaks are much smaller in comparison with Cu-Au(111) system, Fig. S4 (ESI†).

4. Conclusions

In conclusion, by employing the electrochemistry-assisted and jump-to-contact based STM-BJ approach, which creates atomic contacts with crystallographic consistency, we have observed a statistical distribution of last-step length of single atom contact at subatomic distance for both Fe and Cu. Up to five and three well-defined peaks on the last-step length histogram were observed for Fe and Cu, respectively, with integral multiples of subatomic distance close to 0.075 nm. The ultrafine structural rearrangement of the contact region is responsible for such a feature, and most likely one of the {111}-equivalent planes in the contact region is glided upon tip stretching with displacement in the direction from the *fcc*-hollow-site to the *hcp*-hollow-site at 1/3 of the regular layer spacing of corresponding metal. It is noteworthy that the observation of such an ultrafine structural evolution feature may depend on the system being studied. Unfortunately, the classical Au nanoconstriction cannot be created by the jump-to-contact STM-BJ because of the lack of a proper substrate substantially more stable than Au.

However, it should be possible for the structural evolution of an Au single contact to be investigated by the soft STM-BJ approach reported very recently by Sabater *et al.*⁴⁰ Our observation can provide a new understanding of and promote further efforts for experimental investigation of the mechanical property of nanocontacts.

Acknowledgements

The authors are grateful to Prof. Yi Luo at University of Science and Technology of China for valuable discussions and Prof. Michael Blackburn of Sheffield University for English improvement. The authors are grateful to one of the reviewer's kind suggestion for improvement of the model. Our gratitude also goes to a reviewer who suggested for modification of Fig. 6. This work is supported by National Science Foundation of China (No. 20973141, 20911130235, 21033007, 20973144, and 21003110), and CONICET PIP: 11220080100983, Secyt-UNC, Program BID (PICT 2006 No 946, and PME 2006 No 01581) from Argentina. O.A.O thanks CONICET for a fellowship.

Notes and references

- 1 R. Landauer, *IBM J. Res. Dev.*, 1957, **1**, 223–231.
- 2 N. Agrait, A. L. Yeyati and J. M. van Ruitenbeek, *Phys. Rep.*, 2003, **377**, 81–279.
- 3 J. H. Tian, Y. Yang, X. S. Zhou, B. Schollhorn, E. Maisonnaite, Z. B. Chen, F. Z. Yang, Y. Chen, C. Amatore, B. W. Mao and Z. Q. Tian, *ChemPhysChem*, 2010, **11**, 2745–2755.
- 4 P. Shi and P. W. Bohn, *ACS Nano*, 2008, **2**, 1581–1588.
- 5 C. J. Muller, J. M. van Ruitenbeek and L. J. de Jongh, *Phys. C*, 1992, **191**, 485–504.
- 6 A. I. Yanson, G. R. Bollinger, H. E. van den Brom, N. Agrait and J. M. van Ruitenbeek, *Nature*, 1998, **395**, 783–785.
- 7 M. L. Trouwborst, E. H. Huisman, F. L. Bakker, S. J. van der Molen and B. J. van Wees, *Phys. Rev. Lett.*, 2008, **100**, 175502.
- 8 M. Tsutsui, K. Shoji, M. Taniguchi and T. Kawai, *Nano Lett.*, 2008, **8**, 345–349.
- 9 J. H. Tian, B. Liu, X. L. Li, Z. L. Yang, B. Ren, S. T. Wu, N. J. Tao and Z. Q. Tian, *J. Am. Chem. Soc.*, 2006, **128**, 14748–14749.
- 10 J. K. Gimzewski and R. Moller, *Phys. Rev. B*, 1987, **36**, 1284–1287.
- 11 J. I. Pascual, J. Mendez, J. Gomez-Herrero, A. M. Baro and N. Garcia, *Phys. Rev. Lett.*, 1993, **71**, 1852–1855.
- 12 L. Olesen, E. Laegsgaard, I. Stensgaard, F. Besenbacher, J. Schiotz, P. Stoltze, K. W. Jacobsen and J. K. Nørskov, *Phys. Rev. Lett.*, 1994, **72**, 2251.
- 13 N. J. Tao, *Nat. Nanotechnol.*, 2006, **1**, 173–181.
- 14 J. Hihath, C. Bruot and N. Tao, *ACS Nano*, 2010, **4**, 3823–3830.
- 15 C. Untiedt, A. I. Yanson, R. Grande, G. Rubio-Bollinger, N. Agrait, S. Vieira and J. M. van Ruitenbeek, *Phys. Rev. B: Condens. Matter*, 2002, **66**, 085418.
- 16 P. Makk, D. Tomaszewski, J. Martinek, Z. Balogh, S. Csonka, M. Wawrzyniak, M. Frei, L. Venkataraman and A. Halbritter, *ACS Nano*, 2012, **6**, 3411–3423.
- 17 S. Csonka, A. Halbritter and G. Mihály, *Phys. Rev. B: Condens. Matter Mater. Phys.*, 2006, **73**, 075405.
- 18 R. H. M. Smit, C. Untiedt, A. I. Yanson and J. M. van Ruitenbeek, *Phys. Rev. Lett.*, 2001, **87**, 266102.
- 19 P. E. Marszalek, W. J. Greenleaf, H. Li, A. F. Oberhauser and J. M. Fernandez, *Proc. Natl. Acad. Sci. U. S. A.*, 2000, **97**, 6282–6286.
- 20 M. Hafner, K. Viljas, D. Frustaglia, F. Pauly, M. Dreher, P. Nielaba and J. C. Cuevas, *Phys. Rev. B: Condens. Matter Mater. Phys.*, 2008, **77**, 104409.
- 21 G. Autes, C. Barreateau, D. Spanjaard and M. C. Desjonqueres, *Phys. Rev. B: Condens. Matter Mater. Phys.*, 2008, **77**, 155437.
- 22 A. I. Yanson and J. M. van Ruitenbeek, *Phys. Rev. Lett.*, 1997, **79**, 2157–2157.
- 23 J. C. Cuevas, A. L. Yeyati, A. Martin-Rodero, G. R. Bollinger, C. Untiedt and N. Agrait, *Phys. Rev. Lett.*, 1998, **81**, 2990–2993.
- 24 M. Brandbyge, K. W. Jacobsen and J. K. Nørskov, *Phys. Rev. B: Condens. Matter*, 1997, **55**, 2637–2650.
- 25 D. X. Wang, J. W. Zhao, S. Hu, X. Yin, S. Liang, Y. H. Liu and S. Y. Deng, *Nano Lett.*, 2007, **7**, 1208–1212.
- 26 D. Sánchez-Portal, E. Artacho, J. Junquera, P. Ordejón, A. Garcia and J. M. Soler, *Phys. Rev. Lett.*, 1999, **83**, 3384–3387.
- 27 D. R. Strachan, D. E. Smith, M. D. Fischbein, D. E. Johnston, B. S. Guiton, M. Drndic, D. A. Bonnell and A. T. Johnson, *Nano Lett.*, 2006, **6**, 441–444.
- 28 M. L. Trouwborst, S. J. van der Molen and B. J. van Wees, *J. Appl. Phys.*, 2006, **99**, 114316.
- 29 Y. Kondo and K. Takayanagi, *Phys. Rev. Lett.*, 1997, **79**, 3455–3458.
- 30 H. Ohnishi, Y. Kondo and K. Takayanagi, *Nature*, 1998, **395**, 780–783.
- 31 Y. Kondo and K. Takayanagi, *Science*, 2000, **289**, 606–608.
- 32 V. Rodrigues, T. Fuhrer and D. Ugarte, *Phys. Rev. Lett.*, 2000, **85**, 4124–4127.
- 33 V. Rodrigues, F. Sato, D. S. Galvao and D. Ugarte, *Phys. Rev. Lett.*, 2007, **99**, 255501.
- 34 T. Leoni, R. Zoubkoff, S. Homri, N. Candoni, P. Vidakovic, A. Ranguis, H. Klein, A. Saul and P. Dumas, *Nanotechnology*, 2008, **19**, 355401.
- 35 T. Kizuka, *Phys. Rev. B: Condens. Matter Mater. Phys.*, 2008, **77**, 155401.
- 36 C. Z. Li and N. J. Tao, *Appl. Phys. Lett.*, 1998, **72**, 894–896.
- 37 F. Q. Xie, R. Maul, S. Brendelberger, C. Obermair, E. B. Starikov, W. Wenzel, G. Schon and T. Schimmel, *Appl. Phys. Lett.*, 2008, **93**, 043103.
- 38 J. Z. Li, T. Kanzaki, K. Murakoshi and Y. Nakato, *Appl. Phys. Lett.*, 2002, **81**, 123–125.
- 39 T.-W. Hwang and P. W. Bohn, *ACS Nano*, 2011, **5**, 8434–8441.
- 40 C. Sabater, C. Untiedt, J. Palacios and M. Caturla, *Phys. Rev. Lett.*, 2012, **108**, 205502.
- 41 X. S. Zhou, Y. M. Wei, L. Liu, Z. B. Chen, J. Tang and B. W. Mao, *J. Am. Chem. Soc.*, 2008, **130**, 13228–13230.

- 42 W. A. Hofer, A. J. Fisher, R. A. Wolkow and P. Grütter, *Phys. Rev. Lett.*, 2001, **87**, 236104.
- 43 J. Liang, L. Liu, Y. Gao, Y. Wei, Z. Chen, X. Zhou, J. Zhao and B. Mao, *J. Electroanal. Chem.*, 2013, **688**, 257–261.
- 44 X.-S. Zhou, J.-H. Liang, Z.-B. Chen and B.-W. Mao, *Electrochem. Commun.*, 2011, **13**, 407–410.
- 45 J. G. Wang, J. Tang, Y. C. Fu, Y. M. Wei, Z. B. Chen and B. W. Mao, *Electrochem. Commun.*, 2007, **9**, 633–638.
- 46 Y. M. Wei, X. S. Zhou, J. G. Wang, J. Tang, B. W. Mao and D. M. Kolb, *Small*, 2008, **4**, 1355–1358.
- 47 Y. C. Fu, Y. Z. Su, D. Y. Wu, J. W. Yan, Z. X. Xie and B. W. Mao, *J. Am. Chem. Soc.*, 2009, **131**, 14728–14737.
- 48 Y. Z. Su, Y. C. Fu, Y. M. Wei, J. W. Yan and B. W. Mao, *ChemPhysChem*, 2010, **11**, 2764–2778.
- 49 Y. M. Wei, Y. C. Fu, J. W. Yan, C. F. Sun, Z. Shi, Z. X. Xie, D. Y. Wu and B. W. Mao, *J. Am. Chem. Soc.*, 2010, **132**, 8152–8157.
- 50 M. G. Del Pópolo, E. P. M. Leiva, M. M. Mariscal and W. Schmickler, *Nanotechnology*, 2003, **14**, 1009–1013.
- 51 M. G. Del Pópolo, E. P. M. Leiva, M. M. Mariscal and W. Schmickler, *Angew. Chem.*, 2001, **113**, 4807–4809.
- 52 M. G. Del Pópolo, E. P. M. Leiva, H. Kleine, J. Meier, U. Stimming, M. Mariscal and W. Schmickler, *Electrochim. Acta*, 2003, **48**, 1287–1294.
- 53 M. G. Del Pópolo, E. P. M. Leiva, H. Kleine, J. Meier, U. Stimming, M. Mariscal and W. Schmickler, *Appl. Phys. Lett.*, 2002, **81**, 2635–2637.
- 54 T. Konishi, M. Kiguchi and K. Murakoshi, *Surf. Sci.*, 2008, **602**, 2333–2336.
- 55 X. L. Li, H. X. He, B. Q. Xu, X. Y. Xiao, L. A. Nagahara, I. Amlani, R. Tsui and N. J. Tao, *Surf. Sci.*, 2004, **573**, 1–10.
- 56 C. Li, A. Mishchenko and T. Wandlowski, *Top. Curr. Chem.*, 2012, **313**, 121–188.
- 57 L. Lu, M. L. Sui and K. Lu, *Science*, 2000, **287**, 1463–1466.